# Simulation of Polarising and Reflector Gratings for High Power mm Waves

*Carsten* Lechte[1,*], *Walter* Kasparek[1], *Burkhard* Plaum[1], *Fritz* Leuterer[2], *Martin* Schubert[2], *Jörg* Stober[2], and *Dietmar* Wagner[2]

[1]Institut für Grenzflächenverfahrenstechnik und Plasmatechnologie IGVP, Universität Stuttgart, 70569 Stuttgart, Germany
[2]Max-Planck-Institut für Plasmaphysik, 85748 Garching, Germany

**Abstract.** High power mm waves for fusion plasma heating need to be elliptically polarised to ensure good absorption in the plasma. In some scenarios, electron cyclotron resonance heating (ECRH) at higher harmonics (X3 and O2) is used, but this has significant shine-through because of low single pass absorption. Grating reflectors at the inboard strike point form a holographic mirror that reflects the beam back into the plasma. This paper investigates the optical properties and ohmic losses of both the polariser and the reflectors with the 3D fullwave code IPF-FD3D. The reflection properties of a reflector for ASDEX Upgrade and the improved ohmic losses of a waveguide polariser were confirmed.

## 1 Introduction

Polarisers for multi-megawatt mm waves are a vital component in fusion plasma heating systems. The usual arrangement consists of 2 planar mirrors with straight gratings of depths $\lambda/4$ and $\lambda/8$ and periods much smaller than $\lambda$. This arrangement can transform any linearly polarised beam into any elliptical polarisation. Depending on the angle of the grooves to the incident plane, cross polarisation is produced in the desired quantity. The grooves themselves also introduce a phase shift between the E and H plane polarisations. It has been shown [1, 2] that the same effect can also be obtained with just two $\lambda/8$ gratings, which already have less ohmic loss than the deeper $\lambda/4$ grooves.

There are many possibilities for the shape of the grooves. For high-power applications, the main concerns are arcing and ohmic losses. The former is mitigated by rounded shapes, the latter by optimising the groove profiles. It has been shown by previous numerical investigations [3] that in general, wide grooves and thin ridges decrease the ohmic losses.

In electron cyclotron resonance heating (ECRH), advanced scenarios involving higher harmonics (X3 and O2) have significant shine-through because of reduced single-pass absorption. In the fusion experiments ASDEX Upgrade and Wendelstein 7-X, mirrors are placed at the inboard strike points which reflect the wave back into the plasma for a second absorption pass. The secondary strike point is situated on some robust section on the outboard side.

In both cases, the geometry requires 3D simulations to assess the optical qualities and the ohmic losses of the components. This is in contrast to the design stage of the components. For the polarisers, a simple mode analysis is sufficient to ascertain the polarisation parameters, and extensive 2D simulations of a single grating period were sufficient to determine the ohmic losses for certain scenarios, but not for arbitrary groove orientations relative to the plane of incidence.

In the case of the holographic reflector design, the optimisation decomposes the beam into many rays and uses a boundary element code to *independently* optimise a large number local gratings for each ray. A global optimisation is infeasible because of the large number of parameters arising from all the combinations of the local parameters. For the same reason, a 3D fullwave treatment is only feasible for verifying a small number of final results.

In the following section, the fullwave code IPF-FD3D is introduced. The polariser simulations are described in Sec. 3 and their results in Sec. 4. The reflectors are treated in Secs. 5 and 6, followed by the conclusions.

## 2 The Fullwave Code IPF-FD3D

The finite difference time domain code IPF-FD3D [4] can simulate wave propagation in arbitrary media and magnetised plasmas in 2D or 3D cartesian grids. Metallic components are modelled as unmagnetised high density plasmas. This method automatically forces the correct boundary conditions at the metallic surface, and the resulting plasma currents give a relative measure of the ohmic losses.

For the plasma case, the code solves the two Maxwell curl equations for $\vec{E}$ and $\vec{H}$ simultaneously with the cold electron equation of motion, which yields the plasma current $\vec{J}$. The plasma density is adjusted to a skin depth of

*e-mail: carsten.lechte@igvp.uni-stuttgart.de

1–2 grid cells.

$$\frac{\partial}{\partial t}E = \frac{1}{\varepsilon_0}\nabla \times H - \frac{1}{\varepsilon_0}J \quad (1)$$

$$\frac{\partial}{\partial t}J = \varepsilon_0\omega_{pe}^2 E - \omega_{ce}J \times \widehat{B}_0 \quad (2)$$

$$\frac{\partial}{\partial t}H = -\frac{1}{\mu_0}\nabla \times E \quad (3)$$

where $\widehat{B}_0$ is the unity vector in the direction of the background magnetic field $B_0$, $\omega_{ce}$ the electron cyclotron frequency, and $\omega_{pe}$ the plasma frequency. No background magnetic field is present in the present simulations. All these quantities can be time and space dependent. The incident Gaussian beams are injected in the $x$-$y$ plane.

## 3 Simulation of Polarising Gratings

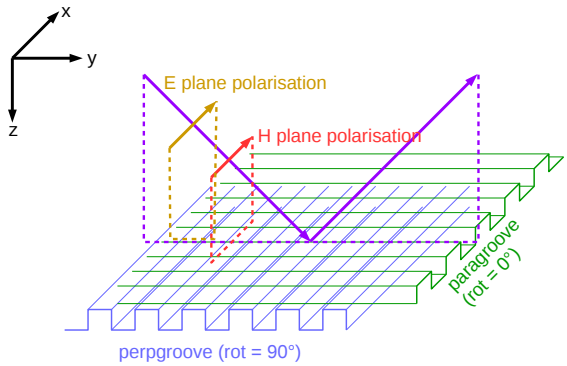


**Figure 1.** Geometry of the polariser simulations. The angle of incidence is always 45°. Simulations are done for E- and H-plane incident polarisation and the groove direction is measured with respect to the plane of incidence, with the 2 extreme cases indicated.

The geometric setup of the polariser simulations is given in Fig. 1. Since the polariser is incorporated into a mitrebend mirror, the angle of incidence is fixed at 45°. The direction of the grooves is chosen to effect the desired polarisation change. From the 2 incident polarisations (E- and H-plane), all elliptical input polarisations can be synthesised by complex linear combination of the complex 3D current distribution. The simulation was run with Gaussian beams with waist size of 4–6 $\lambda$. The spatial grid resolution was 186 points per wavelength, in order to accurately model the sub-mm shape of the grooves.

In addition to the conventional sinusoidal groove shape, the optimised profile "E8_4", developed at IGVP and shown in Fig. 2, was simulated. Basically, the groove width is increased and the ridge width is decreased, and finally the corners are rounded with an exponential function to avoid arcing. An additional constraint of high-power applications is the cooling of the ridges, which must therefore have a minimum width.

In Fig. 3, the electric field strength is shown in the plane perpendicular to the grooves.

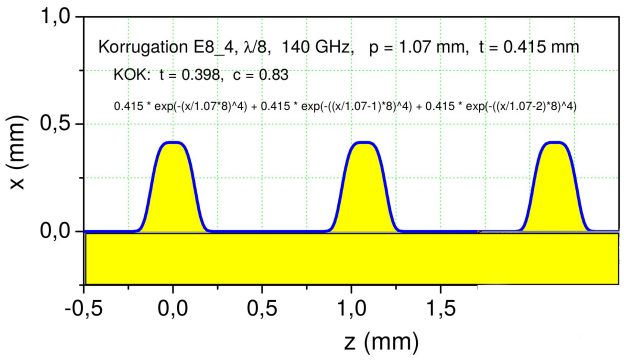


**Figure 2.** Side view of the optimised polariser profile "E8_4" with period $p = 1.07$ mm and ridge height $t = 415\,\mu$m. The equivalent rectangular groove parameters are reduced depth $t$ and groove width $c$ (second line).

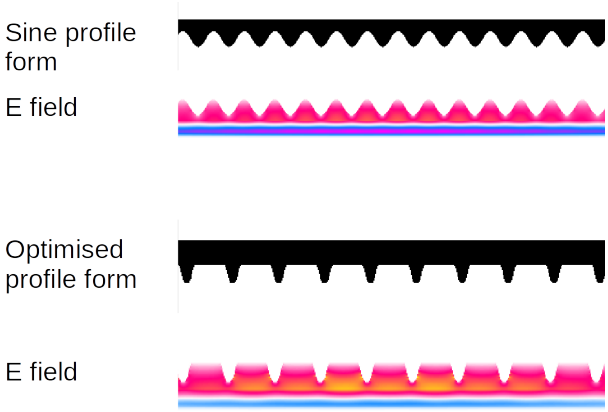


**Figure 3.** Electric fields in the polariser grooves for the sinusoidal and the optimised "E8_4" grating.

## 4 Results for Polarising Gratings

Fig. 4 shows the losses for $\lambda/8$ grooves perpendicular to the plane of incidence. They are normalised to the ohmic losses of perpendicular incidence on a plane mirror. The losses are maximal for E plane polarisation, where the wave can penetrate into the grooves and excites mostly the currents in the $y$ and $z$ directions. For H plane incidence, the $E$ field is parallel to the grooves ($x$ direction) and practically "sees" a slightly bumpy plane mirror. Consequently, the losses are caused only by currents in the $x$ direction ($J_x$). For E plane incidence, the $E$ field is equally distributed between $E_y$ and $E_z$, and the losses for the sinusoid groove shape reflect this equipartition. In the optimised grating, which incidentally has more illuminated surfaces parallel to $y$ (and $x$), more of the losses are carried by currents in the $y$ direction.

Overall, the losses for polarisations near the E plane are reduced by about 20 % for the optimised groove profile. For the case of grooves parallel to the plane of incidence, not shown here, a similar improvement is seen near the H plane polarisation. The simulation results have been confirmed to within 15 % by measurements at ASDEX Upgrade [1, 2].

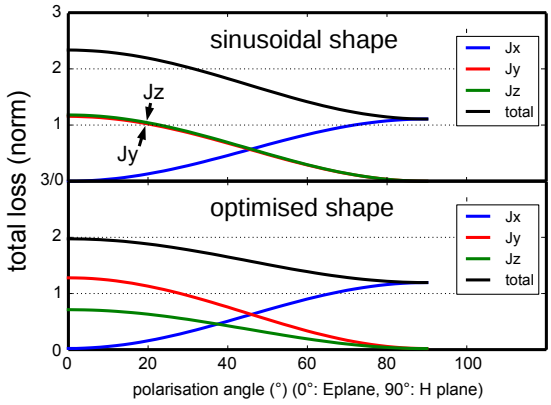


**Figure 4.** Losses of the 2 grating shapes for all linear polarisation angles illuminating grooves perpendicular to the plane of incidence. Losses are normalised to perpendicular incidence on a plane mirror.

## 5 Simulation of Holographic Gratings

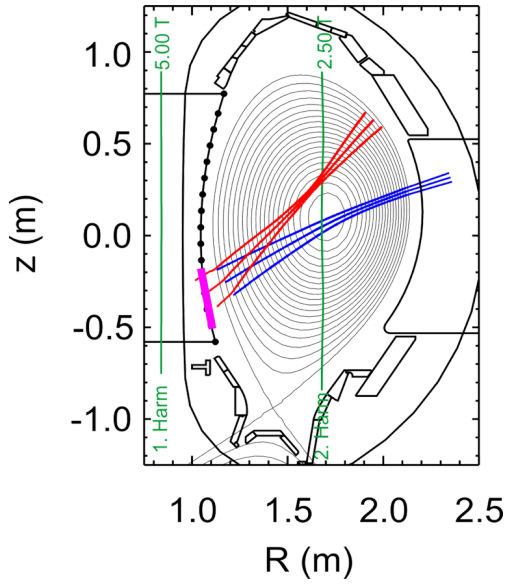


**Figure 5.** Setup of one of the reflecting tiles for ECRH in ASDEX Upgrade. The blue beam is coming from the launchers, and the red beam is reflected into the plasma.

The geometric setup of the reflector simulations is given in Fig. 5. The reflector tile has to conform to the vessel wall and therefore cannot be a simple geometric focussing mirror. Typically, a grating is used to diffract the incident beam into the -3rd to -6th order and to refocus it, preserving the incident polarisation. The term holographic mirror is also used for this component. The grating period is much larger than the one for the polarisers. The design of the grating shape is non-trivial because of the requirement to conserve the incident polarisation. The design process is detailed in the literature [5–7]. The finished tile was checked on the bench [8]. Previously designed tiles have been in operation at ASDEX Upgrade for years.

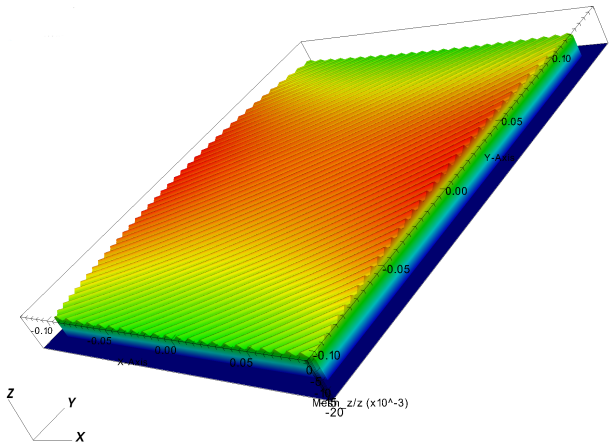

**Figure 6.** Shape of the holographic grating tile R7 for ASDEX Upgrade used in the simulation.

In addition, the properties are checked in a fullwave simulation using both the optimised grating shape (shown in Fig. 6) and the astigmatic elliptically polarised incident Gaussian beam. The simulation covers the full size of the grating tile with a spatial resolution of 20 points per $\lambda$. The incident wave is inserted into the grid in an $x$-$y$ plane at $z$=5 mm. It radiates unidirectionally in the $+z$ direction. The reflected wave can be observed in the $x$-$y$ planes with $z$ <5 mm.

## 6 Results for Holographic Gratings

The wave fields are shown in Fig. 7. The components $E_y$ and $H_x$ were chosen as representative and plotted in the $x$-$z$ an $y$-$z$ planes. Both slices go through the centre of the simulation region. The grating itself is the white shadow at the top of the plots. Positions with $z$ >5 mm show the total field (incident + reflected), and only the reflected field is shown for $z$ <5 mm.

The two top plots show the $x$-$z$ plane. The incident beam is tilted in to $-x$ direction. It can be seen from the interference pattern and from the pure reflected field in the lower part of the plot that the reflected beam is nearly directly reflected into itself in $x$, as designed. The $E_y$ component, being tangential to the groove surface, is 0 at the grating interface. The two bottom plots show the $y$-$z$ plane. The incident beam tilts to the $+y$ direction, and the reflected beam has a much larger tilt, as designed.

The wave field is analysed with plane wave decomposition, shown in Fig. 8. It was taken in the total field region and therefore shows both beams. The incident beam at $k = (-15.0, +8.9)\,\mathrm{cm}^{-1}$ is the same as the design input beam within the simulation grid resolution (because it was put in that way). Its astigmatic nature is apparent in the elliptical shape of the peak.

The reflected beam is at $k = (+14.4, -14.4)\,\mathrm{cm}^{-1}$, which conforms to the design parameters to within 0.2 %. As sketched in Fig. 5, the beam should be reflected, but not directly back into itself. The peak's elliptical shape is stretched and rotated, but this in itself is not a problem

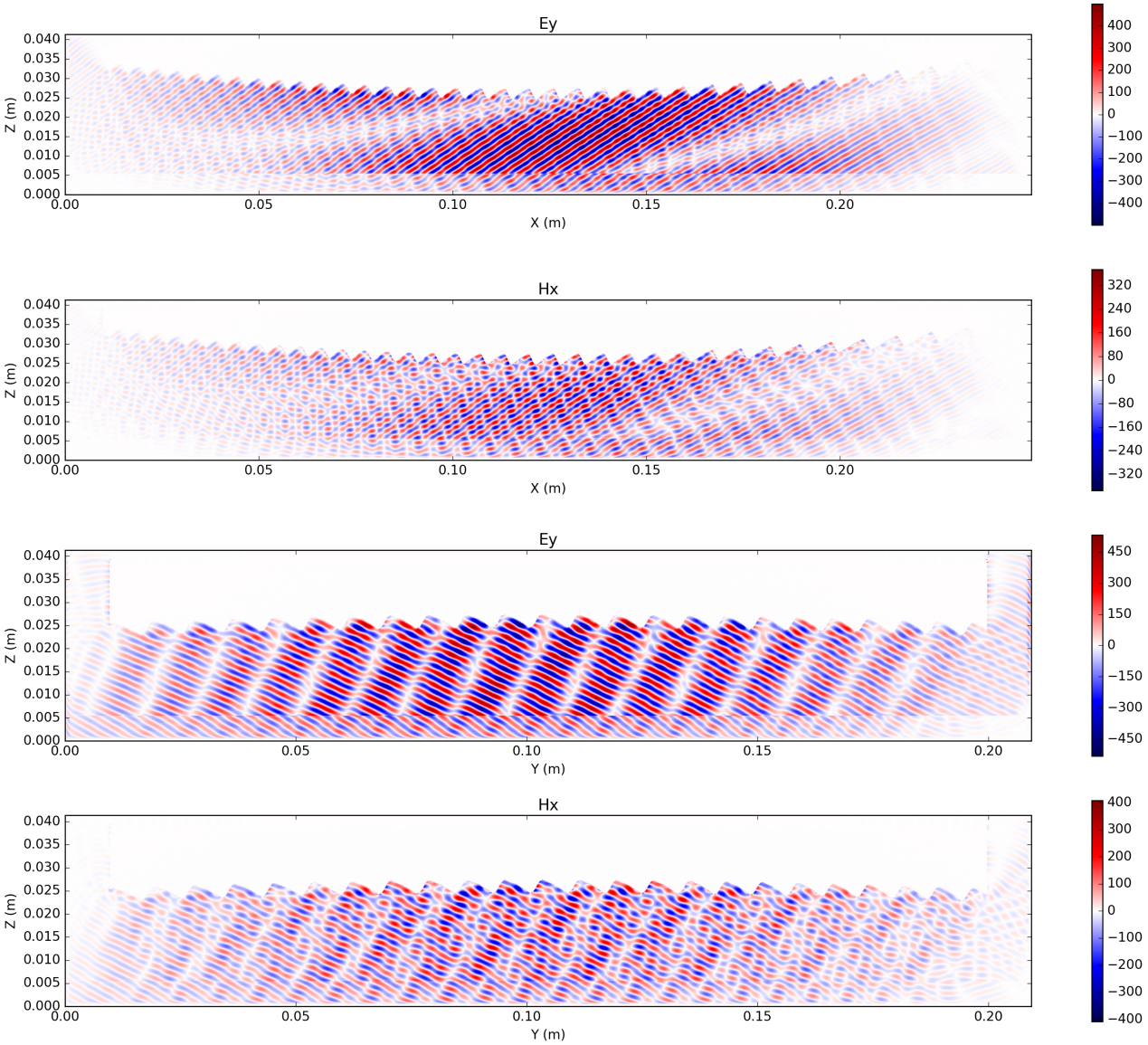


**Figure 7.** Wave $E_y$ and $H_x$ fields in the $x$-$z$ (the two top plots) and $y$-$z$ (two bottom plots) planes. The grating itself is the white shadow at the top of the plots. The incident wave is injected unidirectionally at $z$=5 mm.

for ECRH beams. The important properties of a heating beam are its (lack of) divergence and its polarisation. The reflected beam is not significantly divergent, which can be eye-balled from the extent of the peak, which is the same as the source beam's.

Even in the optimised grating, some percent of the power will inevitably go into unwanted diffraction orders, usually lower ones. One such order is just visible in the plot at $k = (4.6, -6.6)\,\mathrm{cm}^{-1}$. This is not problematic, since the power level is low and the beam will still hit the bulk plasma.

## 7 Conclusions

The application of the 3D fullwave code IPF-FD3D to two important beam forming components for ECRH has confirmed both the loss properties of polariser gratings, and the reflection properties of holographic mirrors gratings designed at IGVP.

For the polarisers, the 3D fullwave simulations have shown a significant decrease of ohmic losses, which was confirmed with high power measurements at ASDEX Upgrade. The optimised groove shape "E8_4" was shown to be advantageous compared to the standard sinusoidal shape.

The holographic grating reflectors for multi-pass ECRH are designed with a numerically intensive optimisation process that only looks at local groove profiles in 2D. For the finished product, a global 3D fullwave simulation is feasible. The imaging properties of the grating were confirmed to a high degree of accuracy. Results of the experimental verification of the manufactured reflecting tile are pending but are expected to support the result of the simulations.

The work was performed within the collaboration with the Max Planck Institute for Plasma Physics (IPP), Garching and Greifswald, Germany.

## References

[1] D. Wagner, F. Leuterer, W. Kasparek, J. Stober, Journal of Infrared, Millimeter, and Terahertz Waves **38**, 191 (2017)

[2] F. Leuterer, D. Wagner, J. Stober, W. Kasparek, C. Lechte, ASDEX Upgrade Team, EPJ Web Conf. **149**, 03002 (2017)

[3] B. Plaum, E. Holzhauer, C. Lechte, Journal of Infrared, Millimeter and Terahertz Waves **32**, 482 (2011), 10.1007/s10762-011-9778-5

[4] C. Lechte, G.D. Conway, T. Görler, C. Tröster, the ASDEX Upgrade Team, Plasma Phys. Contr. Fusion **59**, 075006 (2017)

[5] B. Plaum, M. Schubert, A. Zeitler, W. Kasparek, C. Lechte, J. Stober, the ASDEX Upgrade Team, EPJ Web Conf. (2018), 20th Joint Workshop on Electron Cyclotron Emission and Electron Cyclotron Resonance Heating

[6] H. Höhnle, J. Stober, A. Herrmann, W. Kasparek, F. Leuterer, F. Monaco, R. Neu, D. Schmid-Lorch, H. Schütz, J. Schweinzer et al., Nucl. Fusion **51**, 083013 (2011)

[7] O. Mangold, Ph.D. thesis, Universität Stuttgart (2009)

[8] M. Schubert, J. Stober, A. Herrmann, F. Leuterer, F. Monaco, B. Petzold, E. Poli, S. Vorbrugg, D. Wagner, EPJ Web Conf. (2018), 20th Joint Workshop on Electron Cyclotron Emission and Electron Cyclotron Resonance Heating

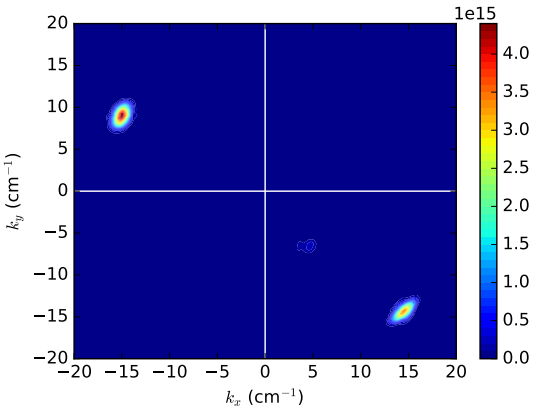


**Figure 8.** Power spectrum of the plane wave decomposition of incident (upper left) out reflected (lower right) wave. A spurious diffraction order is just visible at $k = (4.6, -6.6)\,\mathrm{cm}^{-1}$.